

LUIZ BANDEIRA BRIDGE: ASSESSMENT OF A HISTORICAL RC BRIDGE

José Sena-Cruz^a, Rui Miguel Ferreira^b, Luís Ramos^c,

Francisco Fernandes^d, Tiago Miranda^e, Fernando Castro^f

^a Assistant Professor, ISISE, Univ. of Minho, Dept. of Civil Engineering, Campus de Azurém, 4810-058 Guimarães, Portugal.

E-mail: jsena@civil.uminho.pt; *Corresponding author*

^b Assistant Professor, C-TAC, Univ. of Minho, Dept. of Civil Engineering

E-mail: rmf@civil.uminho.pt

^c Assistant Professor, ISISE, Univ. of Minho, Dept. of Civil Engineering

E-mail: lramos@civil.uminho.pt

^d Assistant Professor, ISISE, Univ. Lusíada, Faculty of Engineering and Technology, Vila Nova de Famalicão, Portugal

E-mail: francisco.fernandes@fam.lusiada.pt

^e Assistant Professor, C-TAC, Univ. of Minho, Dept. of Civil Engineering

E-mail: tmiranda@civil.uminho.pt

^f Full Professor, CT2M, Univ. of Minho, Dept. of Mechanical Engineering, 4810-058 Guimarães, Portugal.

E-mail: fcastro@dem.uminho.pt

Abstract (100-200 words):

The Luiz Bandeira Bridge is located along the Portuguese national road EN333-3, breaching the valley of the Vouga River, just northeast of the small village Sejães, in the district of Oliveira de Frades. It is considered to be the oldest concrete bridge in use in Portugal, and one of the oldest in Europe. Since this bridge is at risk of disappearing due to a construction of a dam, the Department of Civil Engineering of the University of Minho decided to launch a comprehensive study of Luiz Bandeira Bridge, in an attempt to preserve the memory of the past cataloguing the heritage for future reference. These studies include historical, geometrical and damage surveys, the physical and chemical characterization of existing structural materials, the assessment of the reinforcement detailing, dynamic characterization by determining the main frequencies and vibration modes and safety level. This work presents a comprehensive overview of the most important results of these studies.

Keywords: RC bridge; Assessment; Material characterization; Mechanical characterization; Inspection; Dynamic Analysis; Safety analysis;

1. INTRODUCTION

The Luiz Bandeira Bridge is located along the Portuguese national road EN333-3, breaching the valley of the Vouga River, just northeast of the small village Sejães, in the district of Oliveira de Frades. It is considered to be the oldest concrete bridge in use in Portugal, and one of the oldest in Europe. Based on the archives of *Fonds Bétons armés Hennebique*, in Paris, this reinforced concrete bridge may have been designed by the engineer Moreira de Sá and was built by engineers & builders Moreira de Sá & Malevez, dealers of the patented Hennebique system in Portugal.

The name of the bridge come from the General Luiz Bandeira de Mello, a distinguished local public figure who, despite living most of his life in London, never forgot his origin and most probably contributed decisively to the construction of the bridge (Pereira 1998).

The Luiz Bandeira Bridge project was problematic from the start, with conflict and miscommunication between Moreira de Sá & Malevez, the Portuguese government, and the engineers from Hennebique's office in Paris (Tavares 2008). The reasons for the location of the bridge are not clear. The need to link villages on either side of the river and to help develop a link between the industrialized cities of Porto and Viseu, are depicted as the main reasons for the selection of its location, however political, geological and geotechnical aspect also figured into the choice as well (Pereira 1998).

According to the "Revista da Obras Publicas e Minas" journal (ROPM 1908) the construction took 3 months and 4 days and the work was completed on September 14, 1907. However, there are uncertainties about the real duration of the construction. For example, part of the formwork (see **Fig. 1a**) for the construction of the arch was washed away by a major flood during 1906 (Tavares 2008) and there are several "working sheets" dated from 1906.

The original bridge was 44 m long and 4.5 m wide, of which 1.50 m were for the two equal sidewalks in either side of the road. The two parallel arches with a rectangular cross-section of 0.30 m by 0.80 m, with a span of 32 m and a height of 6.4 m, are supported at each end by abutments directly casted on the rock. These arches are connected together by a set of cross beams with a square cross-section of 0.20 m wide. The deck of the bridge is supported by two longitudinal beams, which are supported at the ends by two abutments of concrete (masonry-surfaced) and by the arch at the mid-span. Between the abutments and the arch a set of columns (0.25 m by 0.25 m of cross-section) additionally support the longitudinal beams. The lateral stability of slender columns is guaranteed by longitudinal and transverse beams with a square cross-section of 0.20 m wide. The original sidewalk thickness was 0.10 m, whereas the deck was 0.12 m. For the construction of the bridge, 16 tons

of Bessemer steel and 60 m³ of concrete was required. The total weight of the deck was approximately 167 tonf and the corresponding imposed design load was about 3.9 kN/m² (ROPM 1908).

The bridge was built mostly by workers living in the vicinity of the structure, mainly women, as shown in **Fig. 1b**. The more specialized carpenters and masons from the region were selected, though some belonged to the construction company Moreira de Sá & Malevez.

The inauguration day coincided with the load test of the bridge, perhaps to demonstrate to those present, some related to politics and to the local or regional government, the qualities and abilities of reinforced concrete. These load tests were supervised by the Committee on Examination of Steel Bridges, confirming the uniqueness of this type of bridge construction. The load tests performed included four independent steps: an uniform load composed of sandbags; filling bridge with horse-drawn carriages; measuring the deflection during the passage of a single horse-drawn carriage; and, for conclusion, a gym session with 50 men to check the vibrations (Tavares 2008).

The bridge was news in the magazine "Le Beton Armé" - number 143 - April 1910. In addition to a brief description of the work, photos were included as shown in **Figs. 1b** and **2a**. Three commemorative steel plates were placed at both ends of the downstream arch, one with the name of the bridge and the other with the name of the builder (as shown in **Fig. 2b**).

As a result of the evolution of transport means over the years from the animal-drawn vehicles to heavy motor vehicles, a significant increase in loads had led to a rapid degradation of the structure. Consequently, the bridge underwent rehabilitation during the year 1951. It consisted of the jacketing (addition of steel reinforcement and a layer of concrete) of the reinforced beams, columns and arches. Special care was taken to maintain the original shape of the bridge (Pereira 1998).

Since this intervention no additional work has been done. The images in **Fig. 3** illustrate the bridge's current state.

There is great difficulty in recognizing the importance of historic reinforced concrete, and to ensure its protection and conservation and to properly define the criteria for its management (Mezzina *et al.* 2010). As a result, there is a serious risk that many structures, rich in technical and architectural value, will not survive. The Luiz Bandeira Bridge is a paradigmatic example. The Ribeiradio – Ermida hydroelectric infrastructure along the Vouga River, which includes construction of a dam, is expected to submerge the bridge (Cunha *et al.* 2008).

In this context, a comprehensive study of Luiz Bandeira Bridge was carried out in an attempt to preserve the memory of the past cataloguing the heritage for future reference. These studies include the geometrical and

damage survey, the physical and chemical characterization of existing structural materials, the assessment of the reinforcement detailing, dynamic characterization by determining the main frequencies and vibration modes and safety level.

The main results obtained from these studies are summarized in the following sections.

2. GEOMETRICAL AND DAMAGE SURVEYS AND GEOLOGICAL CHARACTERIZATION

Fig. 4 includes the original (archives of *Fonds Bétons armés Hennebique*) and current geometry of the bridge.

The geometrical survey of the current state was performed by laser distance meter, tape measure, camera and ruler and was compared with the existing drawings from EP (Estradas de Portugal, S.A. - road authority in Portugal, 1995) and the original drawings. No significant discrepancies were noted between the geometrical surveys performed and those of EP. Several discrepancies in terms of the geometrical cross-sections were found when the geometrical survey performed was compared with the original drawings. This was expected since the bridge was submitted to rehabilitation in 1951, as mentioned previously.

During the course of the damage mapping and condition assessment of the bridge, several prevalent degradation mechanisms were observed. The main damage inducing aspects identified are:

- Biological growth (**Fig. 5a**);
- Corrosion of reinforcement and loss of concrete cover due to spalling (**Fig. 5b**);
- Leaching and deposition (**Fig. 5c**);
- Poor detailing and faulty drainage systems; (**Fig. 5d**).

The bridge is subject to extensive biological growth due to the ideal conditions to the development of these organisms. The biological growth observed at the bridge included: algae, moss, lichens and higher plants. In particular, the columns and mid height transverse beams are in good condition with only some biological growth and leaching present.

The deck slab and ribs are generally in poor condition with extensive areas of cracking and exposed corroded, reinforcement. Spalling is an indirect effect caused by the reinforcement expansion due to corrosion. There are also problems with non-structural components, namely metallic elements embedded into concrete with no corrosion protection and leaking water pipes. Moreover, poor detailing of non-structural components were also found for instance iron pipe mountings embedded directly into concrete with no protection.

In the vicinity of the bridge, the geology is mainly characterized by a schist-quartzitic complex and granites of the hercinic period. Near the bridge a medium grain, both biotitic and moscovitic granite rock mass

exists. It is known that this granite was used as aggregate and masonry for the bridge. In the scope of the construction of the Ribeiradio – Ermida hydroelectric infrastructure extensive geological-geotechnical surveys were carried in the area near the bridge. They showed that typically the geomechanical quality of the rock mass increases with depth.

The bridge was built over shallow foundations. The granite rock mass interesting the bridge foundations presents low to medium weathering and fracturing degrees which can be observed in many outcrops at the surface. This fact points out to a reasonable to good geomechanical quality of the rock mass in which the foundations of the bridge were built.

3. MATERIAL CHARACTERIZATION

3.1 Concrete

The characterization of the mix design, composition, physical and mechanical performance of the concrete was based on the testing of concrete cores taken from 20 different locations representing all types of structural elements. The bridge had to remain open to traffic therefore limiting the number of cores taken. In **Fig. 4(b)** the location of the extracted cores can be seen (red circles).

3.1.1 Mix design and composition

Two concrete cores taken from the structure were used to analyse the composition of the original concrete (see **Fig. 6**). The samples were analysed so as to determine the binder/aggregate relationship, the chemical composition of the binder and the aggregate, and the granulometric distribution of the aggregate. The coarse aggregate was not analysed. A detailed description of the quantitative and qualitative characterization methodology can be found in (Ferreira *et al.* 2011). X-ray fluorescence spectrometer and scanning electron microscope with energy dispersive spectroscopy were used to determine the chemical composition of the constituents of the concrete.

The binder/aggregate relationship was determined to be approximately 1:6.5. For sample C7 and C11, approximately 86.4% and 87.1 % by weight of the sample was aggregate, respectively. In **Table 1** the result of the granulometric analysis of the sand is given. A detailed description of the chemical composition as a function of the size of aggregate can be found in (Ferreira *et al.* 2011).

Figs. 7 and **8** illustrate the SEM-EDS images observed with indication of the mineralogical constituents for aggregate fractions greater than 1.4 mm and smaller than 0.75 mm, for the sample C7 and C11, respectively.

In **Figs. 7(a)** and **8(a)**, grains of quartz and mixed grains of potassic feldspars and sodic feldspars can be found.

In the finer fractions of both samples, in addition to the abundant quartz, and to a lesser degree, potassic feldspar, other particles such as iron oxide and aluminium-iron-silicon titanates were found, as shown in the EDS spectrum (**Fig. 9**).

The results of the X-ray diffraction chemical analysis for each of the binder samples are given in **Table 2**. The results indicate that the binder used was a Portland cement. In **Table 3**, the chemical compound composition of the main crystalline phases of cement determined using Bogue's equations (1947), is given.

Both samples show similar chemical composition. **Fig. 10** shows a SEM image in which two main phases in the binders have been identified: tri-calcium silicate (Z1) and bi-calcium silicate (Z2).

3.1.2 Mechanical and physical laboratory tests

The mechanical properties tested from the concrete cores samples were the modulus of elasticity and the compressive strength of concrete according to LNEC E397:1993 and NP EN 12390-3:2003, respectively.

The physical properties tested were the depth of carbonation, porosity and density according to the standards LNEC E391:1993, and LNEC E395:1993. In addition, the thickness of new concrete placed during the rehabilitation in the 1950 was measured. **Fig. 11** presents an overview of the tests performed.

In **Table 4** the results of the mechanical properties tested as well as the thickness of the new concrete are presented. Given the reduced thickness of the concrete used for rehabilitation it was not possible to determine its mechanical properties. In this table E_{cm} and $f_{cm,cyl}$ are the modulus of elasticity and compressive cylinder strength, respectively. In general, the deck is the structural element with the weakest concrete quality. All other structural elements have an average elasticity modulus of approximately 30 GPa and a compressive strength class of at least C30/37. The exception is the deck concrete where the low compressive strength class obtained was due to the large value of the standard deviation.

The porosity of the concrete varies significantly according to the type of structural element. The high porosity obtained is expected due to the probable lack of workability of the fresh concrete and because of the manual compaction techniques that were used. The bridge deck is the element with the highest porosity (11 %) and therefore the lowest specific mass (2287 kg/m³). On the other hand, columns and beams have a lower porosity (approximately 7%) and a higher specific mass (2326 kg/m³). These characteristics are reflected in both the mechanical properties of the concrete as well as in the carbonation depths.

The results for carbonation reflect those obtained for porosity. The carbonation depth for the original concrete deck varied between 110 mm and 130 mm. For the remaining structural elements, the depth of carbonation is almost null. This leads to believe that part of the original concrete cross sections was removed during rehabilitation. The concrete used for the rehabilitation showed depths of carbonation between 2 and 30 mm.

3.2 Steel

3.2.1 *In situ non-destructive tests*

In face of the complexity of existing reinforcement in the bridge, different methodologies for its inspection were used, namely a rebar detector, a georadar and through opening windows allowing a direct observation of the steel mesh. The areas where the nondestructive tests were performed (see **Fig. 12**) were chosen based on the locations where the knowledge of the rebars was relevant for the characterization of the global structural system, as well as in specific zones characterized by peculiar or complex parts of the Hennebique technique (Mezzina 2010). Two nondestructive techniques were used, mainly: a rebar detector using the principle of magnetic induction (Hilti PS 200 Ferroskan®), marked in red dots in **Fig. 12**, and a georadar equipped with an antenna of high frequency (RAMAC/GPR of the MALA Geoscience Inc. with a 1.6 GHz antenna), marked in blue dots in **Fig. 12**. The two techniques had been used in diverse ways in order to optimize the data gathered, as well as to collect as much information as possible at each location.

The results from the two adjacent faces of the same column (positions 1 and 2) and the beam of position 4 from the rebar detector are presented in **Fig. 13**. In these pictures the reconstitution of the existing rebars are presented, namely: the location of the rebars, both principal and stirrups, and an estimative of the concrete cover and the rebar diameter. Relatively to the values of the diameter, it was found that the reinforcement by the use of jacketing is constituted by a longitudinal rebar in the four corners, with a similar diameter in both beams and columns between 16 and 20 mm, and a series of stirrups apart by 10 mm, approximately. The concrete cover at the level of stirrups is around 22 mm with coefficient of variation (CoV) equal to 27%, while being 51 mm (CoV=14%) in the longitudinal ones.

The bridge deck was also inspected (see position 5 in **Fig. 12**). Due to the larger area of inspection, two grids, adjacent to each other, were positioned transversally to the one of the lateral beams (see **Fig. 12**). Each grid was acquired individually and, afterwards, the software joined all the information to produce the map

illustrated in **Fig. 14**, representing the inferior reinforcement from the bridge deck. One can observe a rather regular spacing between the rebars in both directions, essentially in the middle of the map.

In general, with this methodology the distribution of reinforcement mesh is obtained in an almost totally automatic manner. Nevertheless, due to the technology behind this detector, magnetic induction, only the first layer of metallic rebars are detected, as it does not allow the detection of additional information regarding deeper objects, beyond the superficial rebar mesh.

This fact can be observed in three areas pointed out in **Fig. 14** where they exhibit a more complex pattern caused by the superimposition of rebars from the deck and from the beams. Additionally, the estimative of the final rebar diameters carried out by the detector exhibits a large uncertainty, verified by the coefficients of variation calculated. Due to the age of the structure (around a hundred years) some elements can already show signs of corrosion, which can in part explain such high variation coefficients. The variation of the concrete cover below the reinforcement was significantly lower, below 20%. Finally, the diameter estimated by the equipment, which is the result of a preliminary manual adjustment of the diameter and the cover thickness, presents two deficiencies: firstly, it increases significantly the thickness of the concrete cover and, secondly, assigns modern commercial diameter for rebar, which may not coincide with the diameters used at the time of construction of this bridge.

The results obtained with the georadar system confirm the results collected with the rebar detector. In this way, simple single profiles were carried out in a column (position 11) and in one of the transversal beams (positions 7 and 8). In the column, tests were conducted on two adjacent sides in an attempt to characterize the reinforcement from two sides, assuming a symmetrical distribution of the rebars. In the beam, tests were carried out in the locations where they were possible. The results are illustrated in **Figs. 15** and **16**, respectively.

Relatively to the profile carried out in position 11 (see **Figs. 15** and **12**), one can observe the reinforcement close to the surface is constituted by rebars, 10 cm apart, with a rather regular cover, with an average thickness around 25 to 30 mm. The radargram on the right shows a slightly smaller concrete cover. The opposite side of the column was detected around 6 ns, which resulted in an average wave velocity around 12 cm/ns. In the radargrams it is still possible to observe a second reinforcement line at 1.5 ns of depth, which seems to correspond to the original reinforcement of the column. This observation allowed to define, through these measurements, a thickness around 5 cm for the jacketing, which was further confirmed by direct measurement on cylindrical samples. With the value of the jacketing it was possible to confirm the dimensions

of the original cross-section of the beam as 22×22 cm, which is rather close from the dimensions in the real project (20×20 cm).

Finally, several wide hyperbolas appeared at round 4 ns, what, in terms of depth, the referred location corresponds to the original reinforcement. These hyperbolas, in a material where ordinary rebar exhibit thinner hyperboles confirm that these signals might be from larger elements embedded in the concrete. As the Hennebique construction system is characterized by large "U" shaped plates within the reinforcement structure, this is probably an evidence of its use in columns also.

The radargrams illustrated in **Fig. 16** represent two profiles carried out from two sides in a transversal beam. The profile carried out from the top shows the jacketing stirrups (10 cm apart), as well as some evidence of the original beam dimensions. In the radargram on the right, additional signals were observed in the center of the beam, which probably represent vertical elements in the original beam, such as a 3rd stirrup.

In the following figures are illustrated the radargrams obtained in the tests carried out in the starting of one of the main arches. In general, in the profile carried out over the upper surface of the arch one can observe the jacketing reinforcement, constituted by regularly spaced stirrups (10 cm apart) and, apparently, with a regular cover thickness. Immediately below was detected a rather strong but irregular signal, parallel to the surface. Although it cannot be clearly defined all the elements that built that signal, it probably correspond to the interface between the old and new concrete. Most probably, to ensure a correct coupling, the old concrete was dented.

Lateral readings were also executed, along the curvature of the arch and horizontally. The resultant radargrams are illustrated in **Fig. 17**. In both the radargrams are evident at a depth of 2 ns the signals coming from the original reinforcement of the structure, which are clearly different from those produced by the rebars from the jacketing layer, exhibiting a wider signal, pointing towards a metallic element larger than an ordinary rebar. However, these signals seem to be further apart than the ones found in the column and beam analyzed. Additionally, the signals appear to be slightly differently spaced in both radargrams. While on the one in the left the signal seems almost continuous, on the right the same signal appear more apart. That difference can be related with the orientation of the characteristic plates. Additionally, in this last radargram it is possible to observe a third layer of signals associated with the original reinforcement in the opposite side of the arch. The signals coming from the original reinforcement are 12 cm apart, approximately, which means that the arch had, originally, a significant concrete cover thickness laterally, around ¼ of the total thickness of the arch, with the current dimensions.

Additional tests were conducted in an attempt to verify what seems to be the real orientation of original stirrups, taking into account the previous findings. Radargrams carried out, in a direction perpendicular to the curvature of the arch showed a signal parallel to the surface, at 16 cm of depth.

The bridge deck was also inspected but, in this case, the tests were carried out over the road pavement and not from below. Several profiles oriented longitudinally and transversally to the road direction were carried out to characterize the reinforcement in concrete elements. The results obtained from a transversal profile are illustrated in **Fig. 18**, and show the average thickness of the concrete elements (≈ 20 cm in the bridge deck) and the longitudinal rebars in the bridge deck slab and the sidewalks. **Fig. 19** illustrates a longitudinal profile over the sidewalk, which allowed the identification of transversal rebars. Due to the fact that sidewalks are mainly consoles, the reinforcement is located on the top, and consisted of a regularly spaced grid of rebars, 10 cm apart in both directions. The concrete cover was regular, around 6-7 cm. In the bridge deck, while it was possible to observe the presence of reinforcement, its resolution was rather low due to the depth at which it is situated, which prevented its total identification. While the signals detected in **Fig. 18** shows hyperbolas separated by 10 cm, only the inferior reinforcement are clearly visible in the radargrams. Therefore, it seems that the reinforcement distribution in the bridge deck was as a regularly spaced grid of rebars, 10 cm apart.

Finally, a special survey was carried out in the structural join in position 3 (see **Fig. 12**). The results were rather unsuccessful in detailing the original reinforcement but, nevertheless, showed that at the time of the reinforcement by jacketing, no reinforcement was introduced in the joint position.

3.2.2 Chemical tests

The steel plate removed from concrete specimen C7 (see section 3.1) was subjected to a chemical analysis by X-ray fluorescence spectrometer and a basic carbon element test. The results are presented in **Table 5**. The carbon content reveals that steel is mild. The sample was then polished and observed in SEM. The micro-structure is typical of a mild steel containing an appreciable amount of manganese sulphide inclusions, as shown in the micrograph obtained (see **Fig. 20**).

4. EXPERIMENTAL DYNAMIC CHARACTERIZATION

To estimate the dynamic parameters, output-only modal identification techniques are widely applied to large civil engineering constructions, such as bridges and towers (Peeters 2000, Peeters and Roeck 1999). In this type of identification, structures are excited with ambient (natural) vibrations, such as the wind load, traffic or even

the human induced vibrations. In this way, the excitation is considered a white noise signal (stationary Gaussian stochastic process) and only the structural response is measured with highly sensitive sensors (normally accelerometers).

Once the dynamic properties of the structure are known, a numerical model (typically a Finite Element Model) can be built to simulate the structure. The mechanical properties of the model should be tuned by a process called Finite Element Model Updating method. In simple terms, this method can update the mass, stiffness and damping of the numerical model in a way that the numerical parameters (frequencies and mode shapes) are close to the experimental ones. Furthermore, with the tuned model seismic analysis can be carried out, as well the detection of weak points in the structure (damage identification).

The experimental dynamic identification of Sejães bridge was carried out aiming to access its structural behavior by means of calibrating a numerical model. During the experimental campaign, two different identification tests were carried out: ambient excitation tests to estimate the natural frequencies, mode shapes and damping coefficients, and free excitation tests to estimate amplitudes for the evaluation of damping at different and higher excitation amplitudes.

4.1 Ambient vibration tests

Eight piezoelectric accelerometers with 10 V/g sensitivity, able to measure 0.07 mg (where g is the gravity acceleration), were used to record accelerations in ten points of the bridge over four testing setups, see **Fig. 22**. As the measurements were carried out using the natural vibration of the structure, for each setup long periods of measurements were recorded (10 minutes), with a sampling rate of 200 points per second (200 Hz).

For data processing, the Enhanced Frequency Domain Decomposition (EFDD) (Brincker *et al.*, 2000) method and the Stochastic Subspace Identification (SSI) method (Peeters 2000, Peeters and Roeck 1999), available from Extractor software ARTeMIS (SVS 2006), were used.

As an example of signals recorded in acceleration sensors, **Fig. 23a** shows the value of the acceleration sensor positioned at point 4 (see **Fig. 22**) in the vertical direction. As can be seen in the excitation signal, there are some transient signals due to the passage of vehicles over the bridge. However, the maximum excitation environment is less than 4 mg.

Fig. 23b presents the results of modal identification method with the SSI, in terms of the stabilization diagram of poles (frequencies) for the first testing setup. On the stabilization diagram it can be seen several

clusters of stabilized poles between 3 and 20 Hz, corresponding to the estimated natural frequencies of the structure.

Table 6 shows that the first 7 mode shapes, frequencies (f) and their damping ratios (ζ). The natural frequencies are well spaced and range from 3.47 to 16.57 Hz. The standard deviation values for frequencies were equal to 0.18 Hz and 0.06 Hz for the EFDD and SSI method, respectively. The very low value for the uncertainties indicates that the estimation is accurate for both methods. The average error between frequency values obtained by the two methods is equal to 0.8%. In terms of modal damping, an average value of 1.35% and 1.97% were obtained for the EFDD and SSI methods, respectively. The average damping coefficient is within the expected value for this type of structures, although the results showed some variability. As for the modal components, two lateral modes, three vertical bending modes and two torsion modes were identified. The first mode shape is in the lateral direction (y). In general, the modes are symmetric or anti-symmetric, but perturbances can be seen on the symmetry, especially on the torsion modes. When compared the modes from the two methods, Modal Assurance Criterion (MAC) values (Allemang, 2003) close to the unit are obtained, indicating a good correlation between the vectors.

4.2 Dynamic tests with vehicle passing over a bump

A vehicle was driven over the bridge at several different velocities to enhance the input vibrations to the structure. The bump with 2 cm thickness was placed at a one third of the bridge span. The weight of the vehicle was approximately equal to 1550 kg. The vehicle was driven at a constant velocity of 20, 30, 40 and 50 km/h. two series of tests were carried out for each velocity.

The damping was estimated by the logarithm decrement method. The sampling frequency was equal to 5000 Hz and the sensors were placed over the bridge according to the last test setup presented in **Fig. 22**.

Fig. 24a presents the time domain response in the vertical direction of the bridge for the case of 40 km/h. It is possible to see the two impulses induced by the vehicle. The damping was estimated by taking the transient response after the last impulse. It should be stressed that the bump tests excited very well the second vertical mode at around 11.30 Hz.

The estimated damping results are presented in **Table 7**, together with the velocity and root mean square (RMS) of the signals. **Fig. 24b** shows the damping variation according to the excitation level by means of the RMS of the signal. The damping values range between 1.65 and 1.98% and varies according to the level of

excitation induced by the vehicle. This observation allows concluding that the bridge has a nonlinear behavior for the damping.

5. NUMERICAL SIMULATIONS

5.1 Calibration of the numerical model

Before the safety analysis, the numerical model was calibrated with the results of experimental dynamic identification. Due to the structural complexity of the bridge, the calibration was done manually, taking into account different conditions for supports and for the connections between structural elements. The Young's modulus from the different parts of the structure (e.g. deck slab, columns, beams and arch) were kept constant. For the optimization, the dynamic Young's modulus $E_{c,d}$ was taking into account by the relation presented by Neville (1997), as presented in Eq. (1):

$$E_{cm} = 0,83 \times E_{c,d} \quad (1)$$

where E_{cm} is the static Young's modulus considered in agreement with the minor destructive tests carried out for the concrete assessment presented in Section 4.1.

The model updating was carried out by minimizing the differences between frequencies and mode shapes. After successive iterations and analysis, the model that best fits the experimental dynamic behavior was the one in which the deck slab, including the sidewalks, and the upper longitudinal beams were simulated with shell elements, while the other structural elements were simulated with beam elements. The sidewalks were connected to the bridge deck by incline connections. The support conditions at the end of the deck slab and on the lower longitudinal beams were simulated with free translation movements along the x direction, free rotation along y direction, and restrained in the other degrees of freedom. For upper longitudinal beams, only the rotation in the y direction was allowed. In the case of the deck slab, only the longitudinal direction was restrained. The later condition significantly changed the natural frequencies of the bridge.

Fig. 25 presents the tune model for the first horizontal mode shape and the first three vertical mode shapes. The relative error for the frequencies values are computed by taking the results from the SSI presented in **Table 6** as reference. As it can be seen, although the mode shape configuration are close to the experimental ones, only the first and the second mode have relative frequency errors lower than 10%, indicating that further optimization analysis is necessary to tune frequencies. Since the numerical mode shape configuration were similar to the estimated and the structure exhibits a high complexity, the results from the calibration analysis were considered acceptable for the safety analysis.

5.2 Safety analysis

Using the calibrated model described in the previous section safety analysis of the bridge was performed following the recommendations of the R.S.A. (1983), NP EN 1990:2009 e NP EN 1991-1-1:2009 and NP EN 1992-1-1:2010 standards. **Fig. 26** includes the structural model adopted for the safety analysis, as well as the structural components studied. The analysis indicated that these elements verify the strength ultimate limit state.

6. CONCLUSIONS

The present work resumes the studies performed on the Luiz Bandeira Bridge, considered to be the oldest concrete bridge in use in Portugal, and one of the oldest in Europe. The analysis' included historical, geometrical and damage surveys, the physical and chemical characterization of existing structural materials, geological context overview, the assessment of the reinforcement detailing, dynamic characterization by determining the main frequencies and vibration modes and safety level.

From the structural material analysis, both the mechanical properties and the durability performance (carbonation) reflect the physical properties of the concrete, namely the high porosity. The porosity of the concrete deck was high (11%) while the remaining concrete elements had an average value of approximately 7%. Strength classes were greater than C30/37 and the average modulus of elasticity was 30 GPa. The exception was the concrete deck in which these values are quite lower. The binder used was a Portland cement, and the binder/aggregate ratio was 1:6.5. The fine aggregate was a quartzitic/feldspathic sand. The steel used for reinforcement was a mild steel with a very low carbon content.

The steel mesh from the jacketing reinforcement and pavement deck was correctly assessed by both nondestructive techniques used, both showing identical information. Additional information regarding the original reinforcement was uncovered by georadar, which detected the presence of larger metallic elements below the reinforcement rebars, especially in the starting of the arches, and the thickness of the jacketing layer.

From the dynamic identification analysis seven mode shapes were accurately estimated on the Luiz Bandeira Bridge. The frequencies range between 3.5 and 16.5 Hz and are spaced. Damping values were sensitive to the level of vibration and a nonlinear relation was observed between these two quantities. Damping ranges from 1.3 to 2%.

A finite element model was tuned to the experimental dynamic response. The model reasonably reproduces the mode shapes and natural frequencies. Further optimization analysis would be required for a better agreement, but due to the structural complexity of the bridge, the model was considered acceptable for the safety

analysis. The safety analysis indicated that the bridge did not present special concerns.

ACKNOWLEDGMENTS

The authors would like to acknowledge the following people, institutions and companies for their support, and who have made this project become reality:

- To Estradas de Portugal, S.A., and in particular to Elisabete Lopes, for providing the drawing of the bridge, and authorizing the *in-situ* studies;
- To Câmara Municipal de Oliveira de Frades, and in particular to Elisa Oliveira, for the assistance in repairing the damage resulting from the extraction of cores, and for the provided elements related to the hydroelectric complex of Ribeiradio – Ermida;
- To Filipe Soares, for the provided elements related to the construction of the bridge;
- To the fire department of Oliveira de Frades, for the assistance in accessing the bridge;
- To the master students Clive Allen, Luana Boromeo, Mir Abdul Kuddus and Márcio Pereira, for their active collaboration in the studies developed;
- To Jorge Gramaxo, from the Hilti company, for participating in the nondestructive tests for reinforcement identification.

REFERENCES

- Brincker, R., Zhang, L., Andresen, P. (2000) "Modal Identification from Ambient Responses using frequency Domain Decomposition", *In Proceedings of the 18th International Seminar on Modal Analysis*, San Antonio, Texas, 7-10 February.
- Cunha, S., Morais, C. (2008) "Aproveitamento Hidroeléctrico de Ribeiradio - Ermida. F - Estudo de Impacte Ambiental. Volume I - Relatório Síntese/Ribeiradio – Ermida hydroelectric infrastructure. F – Study of environmental impact. Volume I – Summary report", Coba Consultores de Engenharia e Ambiente, July, 647 pp. (in Portuguese)
- EN 1990 (2002) "Eurocode - Basis of structural design." European Committee for Standardization, Brussels.
- EN 1991-1-1 (2002) "Eurocode 1: Actions on structures - Part 1-1: General actions - Densities, self-weight, imposed loads for buildings." European Committee for Standardization, Brussels.
- EN 1992-1-1 (2004) "Eurocode 2: Design of concrete structures - Part 1-1: General rules and rules for buildings." European Committee for Standardization, Brussels.
- Ferreira, R.M., Sena-Cruz, J.M., Castro, F., Abreu, M., Carneiro, L., Castro, F. (2011) "Caracterização do betão da Ponte Luiz Bandeira em Sejães/Concrete characterization of Luiz Bandeira bridge", *In Proceedings of ASCP2011 – 2nd Conference on Safety and Maintenance of Bridges*, University of Coimbra, June 29 – July 1, Coimbra, Portugal, 515-522. URI: <http://hdl.handle.net/1822/12811> (in Portuguese)
- LNEC E391-1993. Betões.Determinação da resistência à carbonatação. Lisboa, Especificação LNEC. (Portuguese specification)
- LNEC E395-1993. Betões. Determinação da absorção de água por imersão. Ensaio no vácuo. Lisboa, Especificação LNEC. (Portuguese specification)
- LNEC E397-1993. Betões – Determinação do módulo de elasticidade em compressão. Lisboa, Especificação LNEC. (Portuguese specification)
- Mezzina, M., Palmisano, F., Uva, G. (2010) "Reinforced Concrete Constructions at the Beginning of the 20th Century: Historical Review and Structural Assessment", *In Proceedings of 2010 Materials, Technologies and Practice in Historic Heritage Structures*, Part III, DOI: 10.1007/978-90-481-2684-2_16, 293-323.
- "Le béton armé en Portugal/The reinforced concrete in Portugal ", *Le Béton Armé Journal*, Paris, 143, April, 1910, 56-59. (in French)
- Neville, A. M. (1997) "Propriedades do concreto/Properties of concrete", Second edition, São Paulo, Pini. (in Portuguese)

NP EN 12390-3:2003. Ensaios do betão endurecido. Parte 3: Resistência à compressão dos provetes de ensaio.

CEN – Comité Europeu de Normalização. Versão Portuguesa: Instituto Português da Qualidade, Caparica, Portugal, 22 pp. (Portuguese standard)

NP EN 13791:2008. Avaliação da resistência à compressão do betão nas estruturas e produtos prefabricados.

CEN – Comité Europeu de Normalização. Versão Portuguesa: Instituto Português da Qualidade, Caparica, Portugal, 32 pp. (Portuguese standard)

Peeters, B. (2000) "System Identification and Damage Detection in Civil Engineering", PhD Thesis, Catholic University of Leuven, Belgium.

Peeters, B.; and De Roeck, G. (1999) "Reference-Based Stochastic Subspace Identification for Output-Only Modal Analysis", *Mechanical Systems and Signal Processing*, 13(6), 855-878

Pereira, M.A.M. (2010) "Estudo da Ponte Luiz Bandeira em Oliveira de Frades – Análise material e estrutural/Study of Luiz Bandeira Bridge – Material and structural analysis", MSc dissertation, Department of Civil Engineering, University of Minho. 130 pp. (in Portuguese)

Pereira, S.M.S. (1998) "Ponte Luiz Bandeira/Luiz Bandeira bridge", Report, School of de Mira, Coimbra, 33 pp. (in Portuguese)

R.H. Bogue, (1947) "Chemistry of portland cement", *Reinhold Pub. Corp.*, New York, pp. 61-67.

R.S.A. (1983) "Regulamento de Segurança e Acções para Estruturas de Edifícios e Pontes", Decreto Lei n.º 235/83, 31 de Maio. (Portuguese standard)

ROPM (1908) "Revista de Obras Publicas e Minas/Journal of the Public Constructions and Mines", Portuguese Association of Civil Engineers, Tomo XXXIX, Lisboa, Imprensa Nacional, pp. 25. (in Portuguese)

SVS (2006): ARTeMIS Extractor Pro User Manual, Release 3.5, Structural Vibration Solutions, Aalborg, Denmark.

Tavares, A.C. (2008) "O Tráfico do moderno/Modern traffic", PhD thesis, Faculty of Architecture, University of Porto, Portugal, 212 pp.

TABLE CAPTIONS

Table 1: Granulometric grading of the sand

Table 2: Chemical composition of the cements (%)

Table 3: Compound composition of cement (%)

Table 4: Mechanical properties of the old concrete and thickness of new concrete

Table 5: Chemical composition of the steel (in percentage)

Table 6: Estimated modal parameters

Table 1: Granulometric grading of the sand.

Fractions	Sample C7	Sample C11
> 1.4 mm	82.4	81.0
> 1.0 mm	5.2	5.9
> 0.5 mm	6.3	6.9
> 0.35 mm	1.6	1.8
> 0.18 mm	2.3	2.4
> 0.075 mm	1.2	1.0
< 0.075 mm	1.0	1.1

Table 2: Chemical composition of the cements (%)

Oxide	C7	C11
CaO	59.2	58.4
SiO ₂	22.6	21.1
Fe ₂ O ₃	5.5	6.4
Al ₂ O ₃	6.1	6.9
MgO	1.0	1.1
K ₂ O	1.2	0.9
Na ₂ O	0.55	0.62
P ₂ O ₅	1.1	1.0
SO ₃	1.1	1.4
TiO ₂	1.1	1.8
MnO	0.19	0.13
SrO	0.22	0.23

Table 3: Compound composition of cement (%)

Compound	C7	C11
C ₃ S	20	18
C ₂ S	49	47
C ₃ A	4	7
C ₄ AF	19	19
Gypsum	2.4	3.0

Table 4: Mechanical properties of the old concrete and thickness of new concrete

Structural element	Average thickness of new concrete (mm)	E_{cm} (GPa)	$f_{cm,cyl}$ (MPa)	Compressive strength class
Arch	55	37.1 (n/a)	59.7 (16%)	C35/45
Column	35	30.4 (21.3%)	51.2 (34%)	C35/45
Deck	90	12.8 (12.8%)	22.7 (15%)	C16/20
Beam (long. & trans.)	40	28.6 (23.0%)	43.6 (24%)	C30/37
Cross beam in arch	40	n/a	24.1 (n/a)	C30/37

Notes: testing performed on specimens with unit height/diameter ratio; cylinder strength class determined according to the NP EN 13791:2008; values in brackets correspond to coefficient of variation; n/a – not available.

Table 5: Chemical composition of the steel (in percentage)

Element	Steel
C	0.03
Mn	0.48
Si	0.04
P	0.067
S	0.050

Table 6: Estimated modal parameters

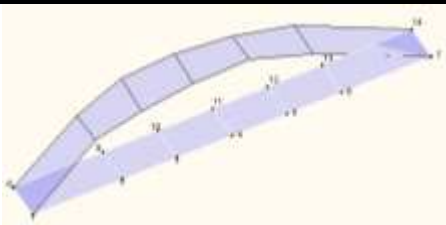
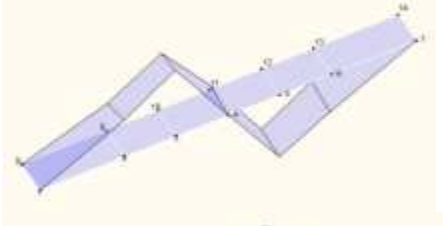
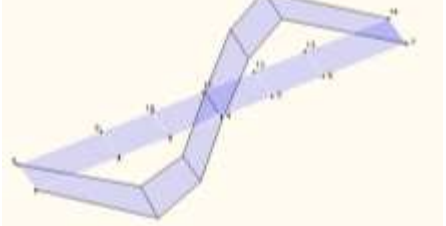
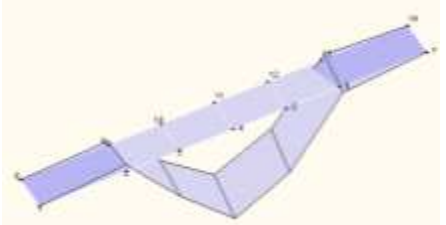

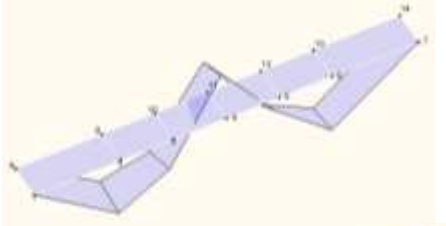
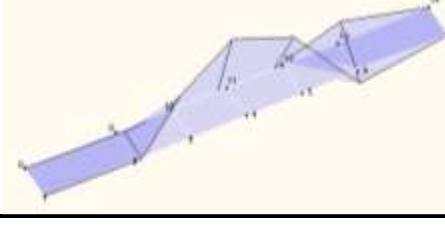
Mode shape	Graphical representation of the modes obtained by the SSI method	Description	EFDD method		SSI method		MAC
			f [Hz]	ζ [%]	f [Hz]	ζ [%]	
1		1 st lateral mode (symmetric)	3.47	1.69	3.47	2.00	>0.99
2		1 st vertical mode (anti-symmetric)	8.08	3.51	7.98	3.06	0.97
3		2 nd lateral mode (anti-symmetric)	9.23	0.40	9.24	1.90	0.85
4		2 nd vertical mode (symmetric)	11.48	1.96	11.45	1.89	>0.99
5		1 st Torsion mode	13.19	0.28	13.16	1.38	0.87
6		3 rd vertical mode (symmetric)	13.90	1.43	13.93	1.34	0.99
7		2 nd Torsion mode	15.97	0.20	16.57	2.21	0.88

Table 7: Damping estimation results

Test	Velocity [km/h]	RMS [mg]	Damping [%]
1	20	6.00	1.65
2	30	13.35	1.72
3	40	16.10	1.78
4	50	18.10	1.98

FIGURE CAPTIONS

Fig. 1: (a) Formwork adopted for the construction of the bridge; (b) workers of the construction.

Fig. 2: (a) Photo of the bridge after its construction, (b) Memorial plate of the construction.

Fig. 3: Views of the Luiz Bandeira Bridge revealing its current state.

Fig. 4: (a) Original geometry (drawings from archives of Fonds Bétons armés Hennebique, 1906); (b) Sketch of the current geometry obtained from the geometrical survey.

Fig. 5: (a) Biological growth (moss) observed on bridge; (b) Concrete spalling and corrosion of the reinforcement; (c) Deposits (leaching) observed on columns; (d) Damage to abutment due to the presence of water.

Fig. 6: Concrete cores taken from bridge. (a) C7 – transversal beam, (b) C11 – bridge deck.

Fig. 7: SEM images of sample C7 - (a) fraction > 1.4 mm, (b) fraction < 0.075 mm

Fig. 8: SEM images of sample C11 - (a) fraction > 1.4 mm, (b) fraction < 0.075 mm

Fig. 9: EDS spectrum for a particle from sample C11 (fraction < 0.075 mm)

Fig. 10: SEM image with atomic contrast showing microstructure of the mortar. Two binder phases has been identified: tri-calcium silicate (Z1) and bi-calcium silicate (Z2)

Fig. 11: (a) View of concrete core after extraction. Note the different type of concretes, and the steel plate reinforcement used in the initial construction; (b) Carbonation depth measurements; (c) Modulus of elasticity testing; (d) Compressive strength testing

Fig. 12: Location of the tested areas and the correspondent techniques

Fig. 13: Results from the tests made with the rebar detector. Column (a) position 1, (b) position 2 and (c) beam, position 4

Fig. 14: Reinforcement mesh obtained from the bottom of the bridge deck (position 5)

Fig. 15: Results from georadar in the column (position 11)

Fig. 16: Results from georadar in one of the transversal square beams (positions 7 e 8)

Fig. 17: Results in the starting of the arch (position 9), laterally

Fig. 18: Results in the bridge deck: transversal test, from sidewalk to sidewalk

Fig. 19: Results in the bridge deck: transversal test, along one of the sidewalks

Fig. 20: Micrograph of the steel

Fig. 21: Dynamic identification tests: (a) detail of the accelerometer; (b) location of the sensors over the bridge; (c) measuring equipment; and (d) free vibration test

Fig. 22: Ambient testing setups: (a) lateral view; (b) plan view; (c) cross section

Fig. 23: Data processing of ambient vibration data: (a) time record for the sensor at position 4 (see Fig. 22); (b) stabilization diagram for Setup 1

Fig. 24: Damping estimation: (a) transient response of the bridge when the vehicle passed with 40 km/h over the bump; and (b) the damping variation according with excitation level

Fig. 25: First four numerical mode shapes (frequency errors are related to the SSI estimation values)

Fig. 26: (a) Structural model adopted for the safety analysis; (b) Structural components analyzed



(a)



(b)

Fig. 1: (a) Formwork adopted for the construction of the bridge; (b) workers of the construction.



(a)



(b)

Fig. 2: (a) Photo of the bridge after its construction, (b) Memorial plate of the construction.



(a)

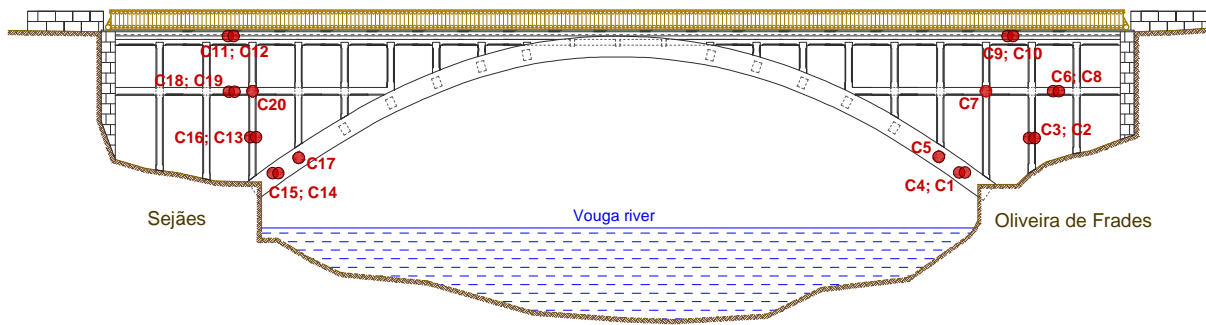


(b)

Fig. 3: Views of the Luiz Bandeira Bridge revealing its current state.



(a)



(b)

Fig. 4: (a) Original geometry (drawings from archives of *Fonds Bétons armés Hennebique*, 1906); (b) Sketch of the current geometry obtained from the geometrical survey.



(a)



(b)



(c)



(d)

Fig. 5: (a) Biological growth (moss) observed on bridge; (b) Concrete spalling and corrosion of the reinforcement; (c) Deposits (leaching) observed on columns; (d) Damage to abutment due to the presence of water.

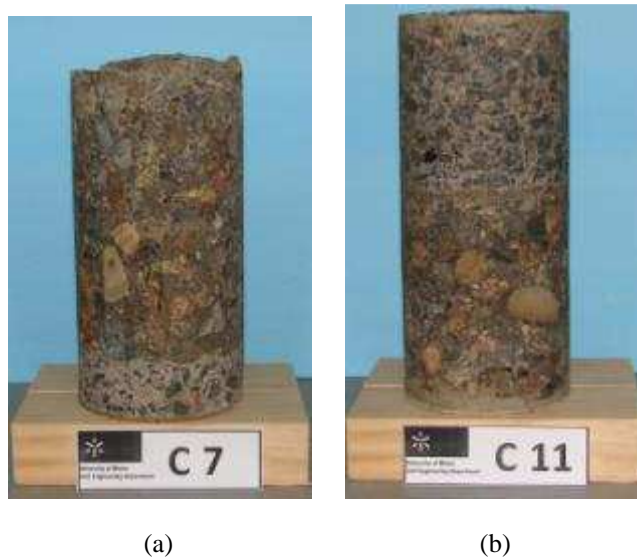


Fig. 6: Concrete cores taken from bridge. (a) C7 – transversal beam, (b) C11 – bridge deck.

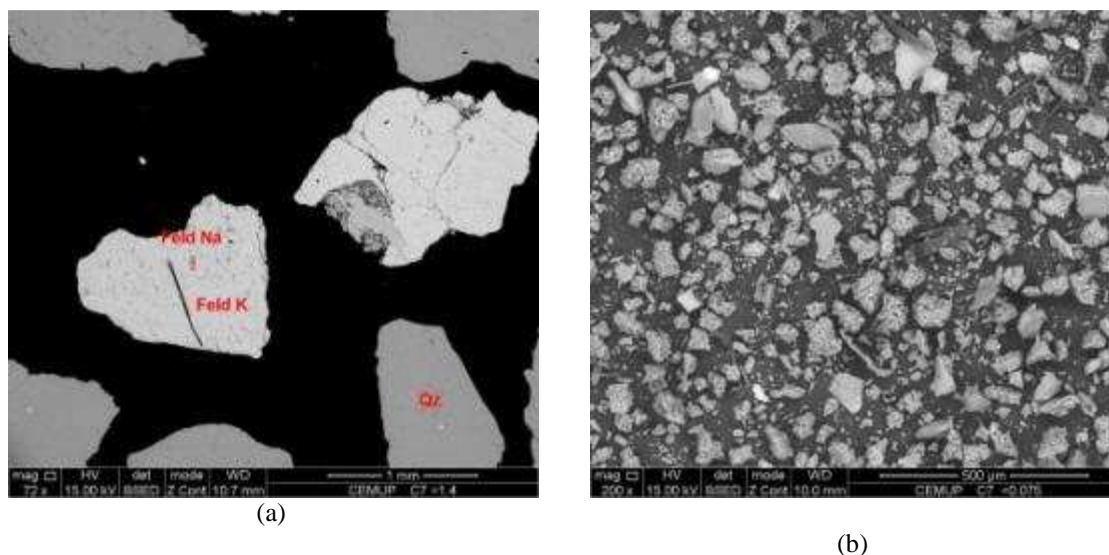


Fig. 7: SEM images of sample C7 - (a) fraction > 1.4 mm, (b) fraction < 0.075 mm

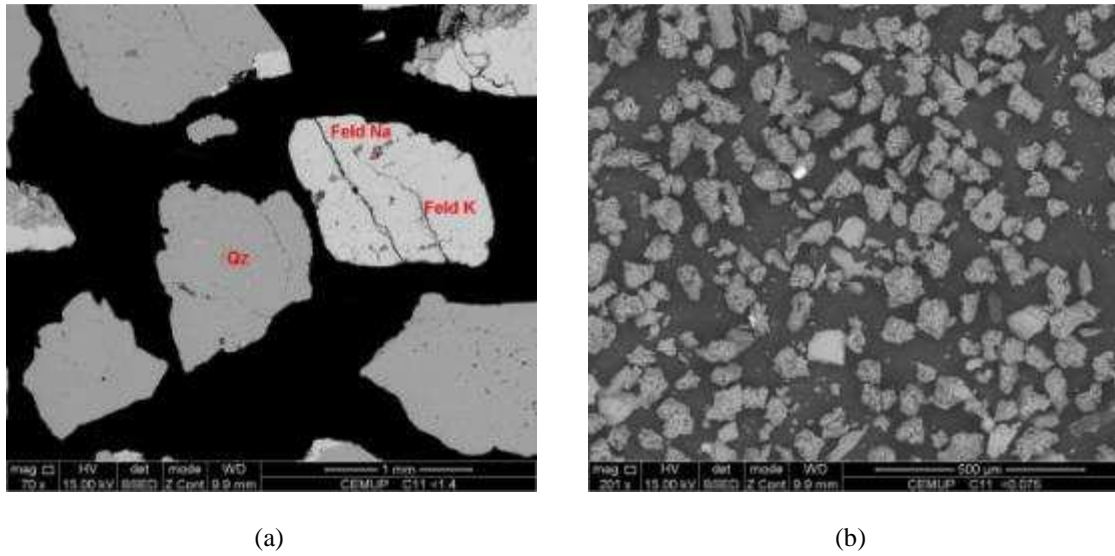


Fig. 8: SEM images of sample C11 - (a) fraction > 1.4 mm, (b) fraction < 0.075 mm

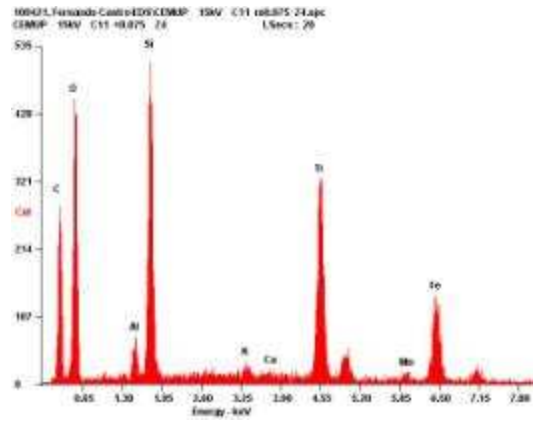


Fig. 9: EDS spectrum for a particle from sample C11 (fraction < 0.075 mm)

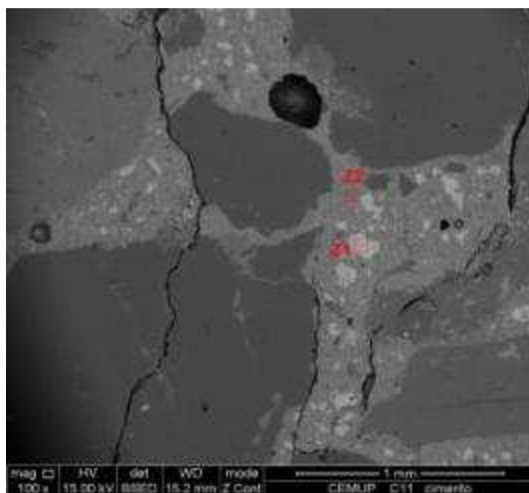


Fig. 10: SEM image with atomic contrast showing microstructure of the mortar. Two binder phases has been identified: tri-calcium silicate (Z1) and bi-calcium silicate (Z2)

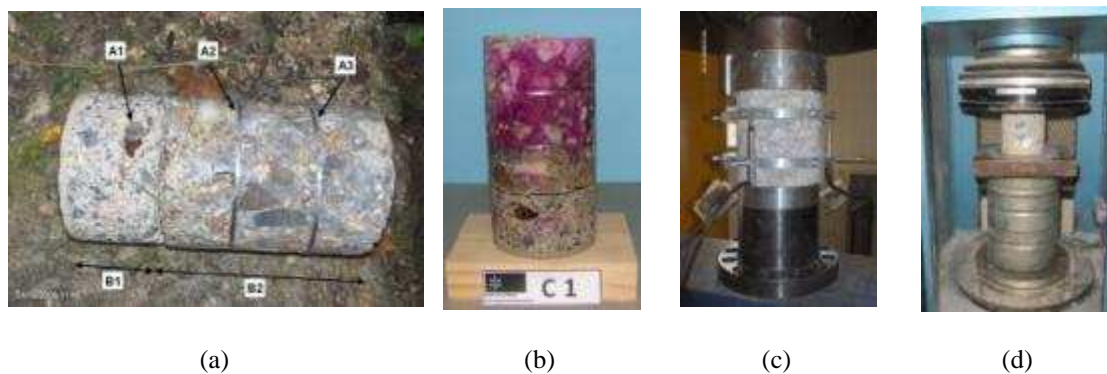


Fig. 11: (a) View of concrete core after extraction. Note the different type of concretes, and the steel plate reinforcement used in the initial construction; (b) Carbonation depth measurements; (c) Modulus of elasticity testing; (d) Compressive strength testing

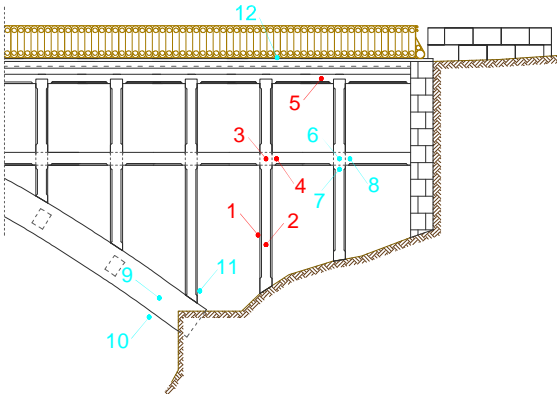


Fig. 12: Location of the tested areas and the correspondent techniques

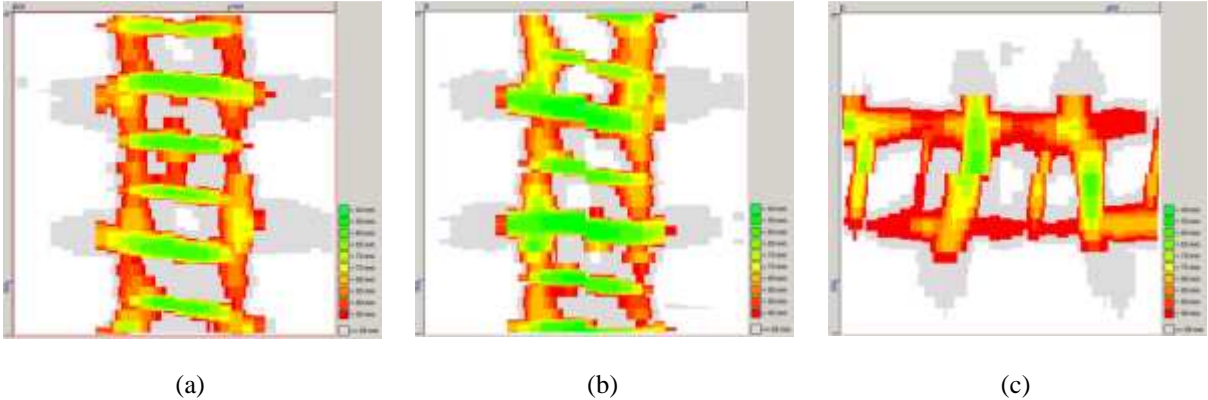


Fig. 13: Results from the tests made with the rebar detector. Column (a) position 1, (b) position 2 and (c) beam, position 4

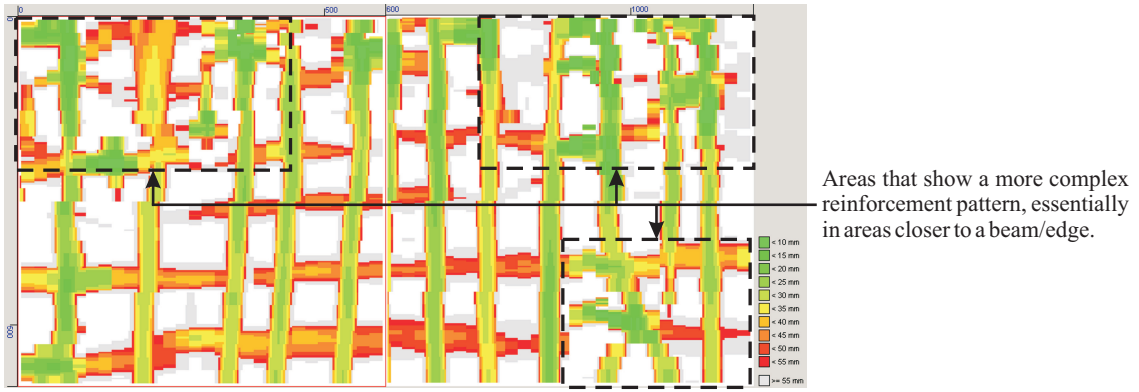


Fig. 14: Reinforcement mesh obtained from the bottom of the bridge deck (position 5)

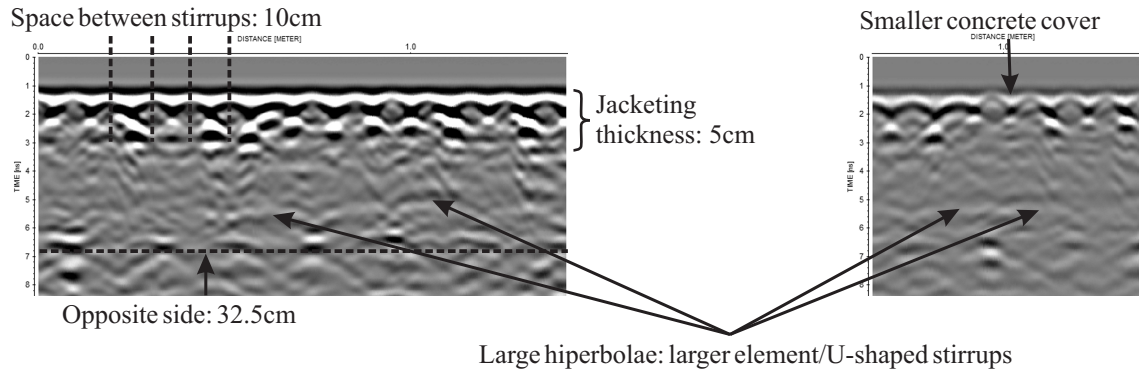


Fig. 15: Results from georadar in the column (position 11)

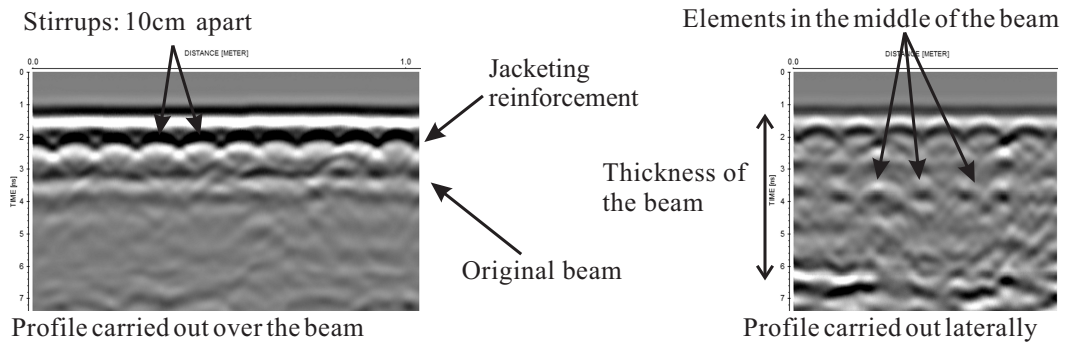


Fig. 16: Results from georadar in one of the transversal square beams (positions 7 e 8)

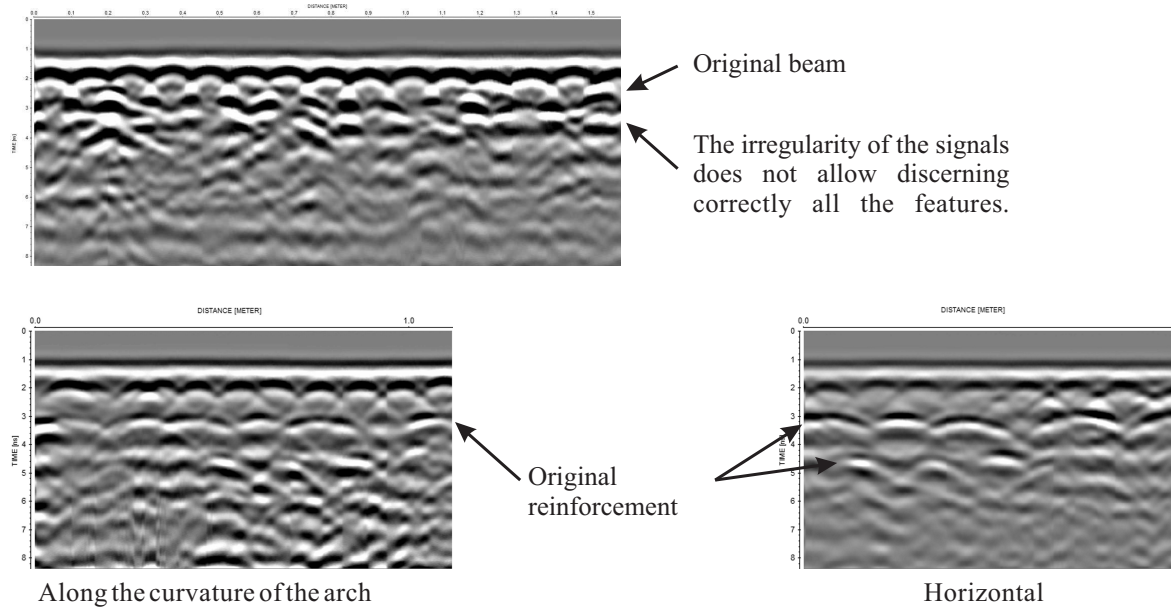


Fig. 17: Results in the starting of the arch (position 9), laterally

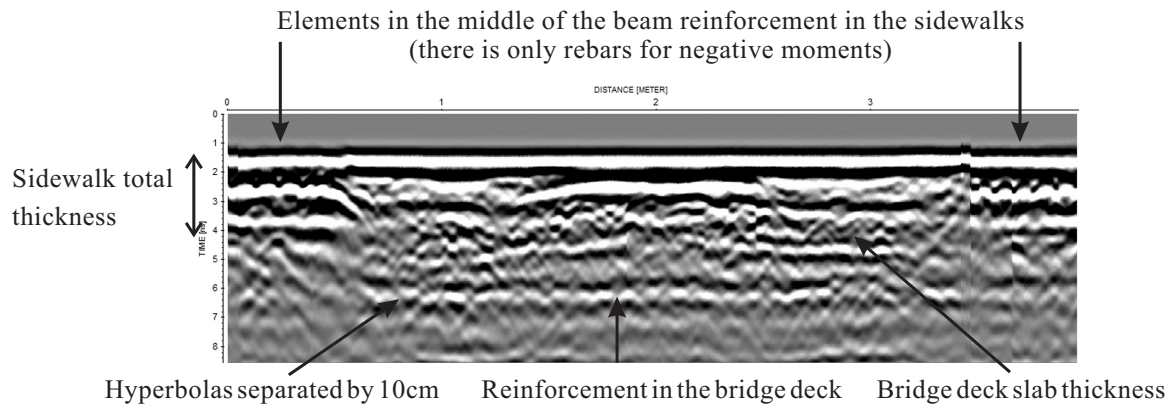


Fig. 18: Results in the bridge deck: transversal test, from sidewalk to sidewalk

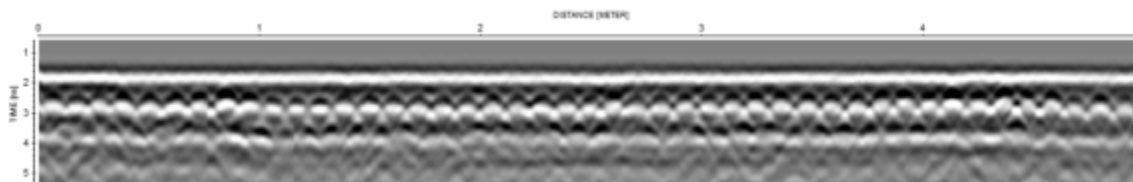


Fig. 19: Results in the bridge deck: transversal test, along one of the sidewalks

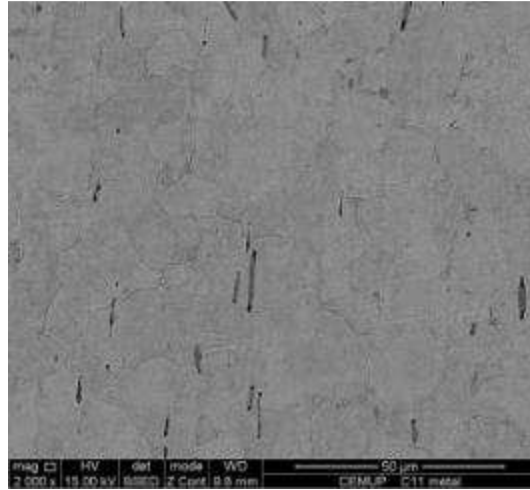


Fig. 20: Micrograph of the steel



(a)



(b)



(c)



(d)

Fig. 21: Dynamic identification tests: (a) detail of the accelerometer; (b) location of the sensors over the bridge; (c) measuring equipment; and (d) free vibration test

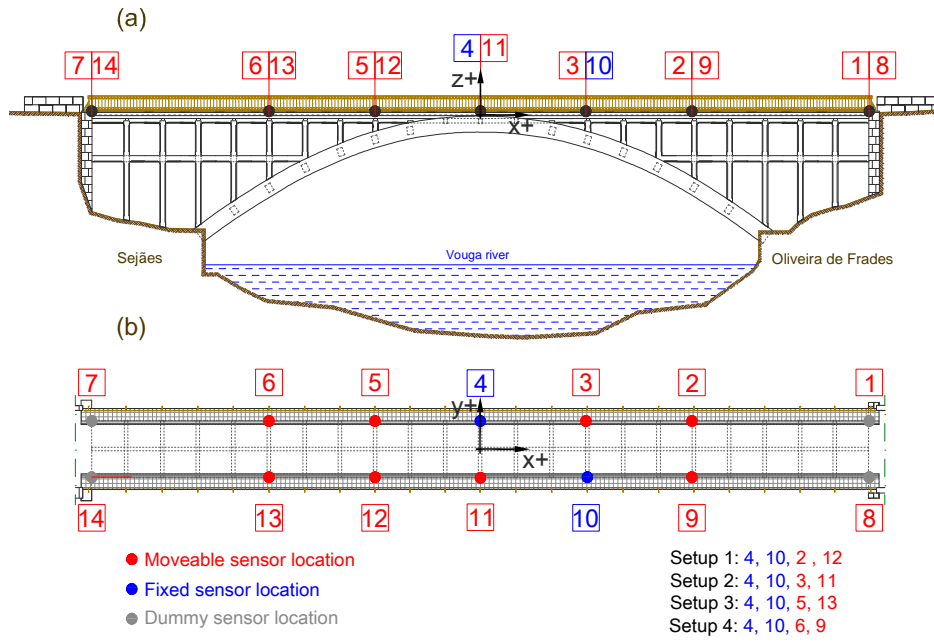
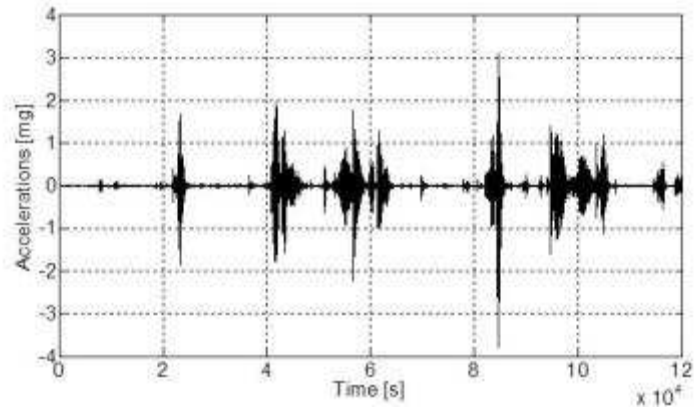
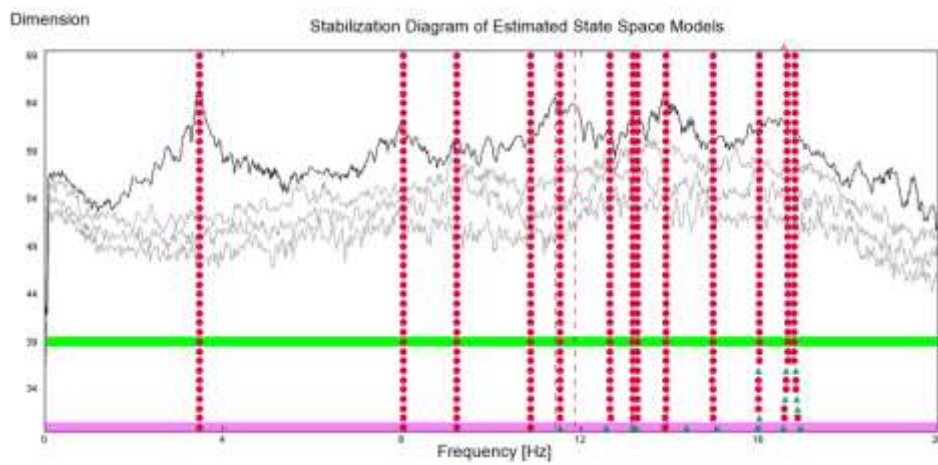


Fig. 22: Ambient testing setups: (a) lateral view; (b) plan view



(a)



(b)

Fig. 23: Data processing of ambient vibration data: (a) time record for the sensor at position 4 (see **Fig. 22**);

(b) stabilization diagram for Setup 1

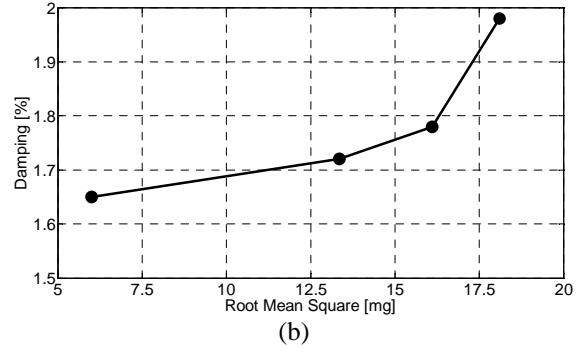
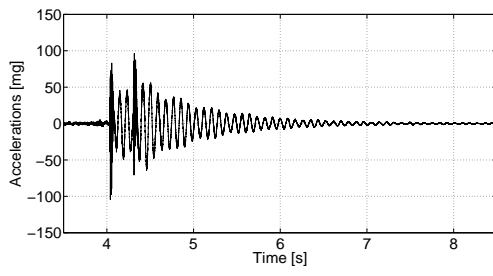


Fig. 24: Damping estimation: (a) transient response of the bridge when the vehicle passed with 40 km/h over the bump; and (b) the damping variation according with excitation level

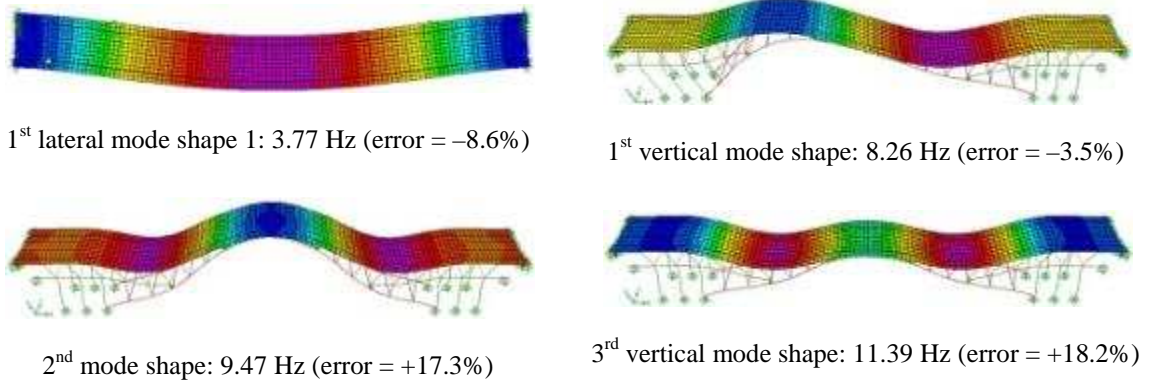
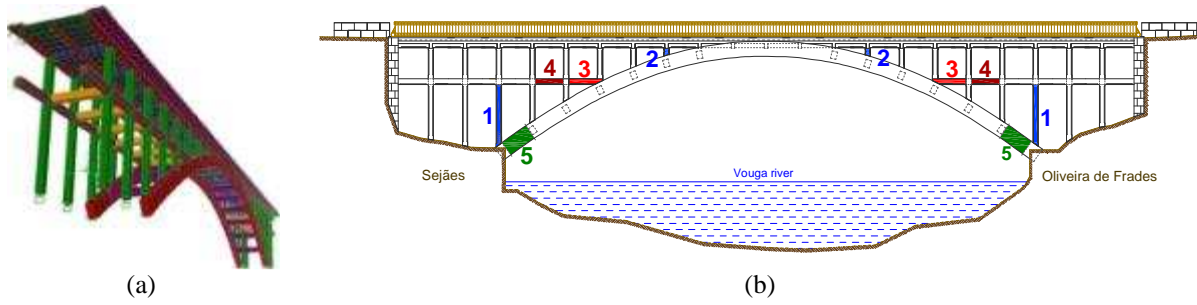


Fig. 25: First four numerical mode shapes (frequency errors are related to the SSI estimation values)



(a) (b)
Fig. 26: (a) Structural model adopted for the safety analysis; (b) Structural components analyzed